GALNet: An End-to-End Deep Neural Network for Ground Localization of Autonomous Cars

Ricardo Carrillo Mendoza[1] [a], Bingyi Cao [1] [b], Daniel Goehring[1] [c] and Raúl Rojas [1] [d]

[1] *Freie Universitaet Berlin, Institut of Informatics, Berlin, Germany*

{*Ricardo.Carrillo, Bingyi.Cao, Daniel.Goehring, Raul.Rojas*}*@fu-berlin.de*

Keywords: Navigation, Odometry, Deep Learning, Autonomous Cars.

Abstract: Odometry based on Inertial, Dynamic and Kinematic data (IDK-Odometry) for autonomous cars has been widely used to compute the prior estimation of Bayesian localization systems which fuse other sensors such as camera, RADAR or LIDAR. IDK-Odometry also gives the vehicle information by way of emergency when other methods are not available. In this work, we propose the use of deep neural networks to estimate the relative pose of the car given two timestamps of inertial-dynamic-kinematic data. We show that a neural network can find a solution to the optimization problem employing an approximation of the Vehicle Slip Angle (VSA). We compared our results to an IDK-Odometry system based on an Unscented Kalman Filter and Ackermann-wheel odometry. To train and test the network, we used a dataset which consists of ten driven trajectories with our autonomous car. Moreover, we successfully improved the results of the network employing collected data with a model autonomous car in order to increase the trajectories with high VSA.

1 INTRODUCTION

Localization is a fundamental requirement for autonomous cars. Vehicles must be able to avoid obstacles by planning safe paths to reach the desired destination in order to operate autonomously.

Odometry methods based on the kinematics of the car mechanical linkages like differential Odometry or Ackermann steering are widely employed in the literature; some examples are (Valente et al., 2019), and (Weinstein and Moore, 2010). Those methods are normally fused with information from an Inertial Measurement Unit (IMU) which also drifts in time due to inaccurate bias estimation or integration. Localization systems which fuse GPS with other sensors have significant limitations associated with the unavailability or highly erroneous GPS based position estimation.

In contrast, the use of vehicle dynamic parameters for localization is relatively rare. Wheel parameters such as rotational velocity or tire force, commonly are used to develop stabilization control systems and Advanced Driver Assistance System (ADAS) through computing Vehicle Slip Angle (VSA)(Chindamo et al., 2018). Estimating the VSA of the vehicle to correct odometry is problematic since it relies on wheel speed readings, if external conditions such as weather, road conditions, tire air pressure, or vehicle weight (due to trunkload or number of passengers) change the dynamics of the car, the estimator is unable to know those changes, and it would lead to big inaccuracies. Parameters such as variable wheel size, different tire materials, spring effects due to the suspension system, diverse steering and traction mechanisms makes it difficult to the estimators achieve the necessary accuracy. Furthermore, some indirect external agents cause wheel odometry to be imprecise, for instance, road conditions, driving habits, weather, variable vehicle weight, components failure, and wear. Therefore, it is necessary to develop a system able to learn how the dynamic-kinematic parameters of the car relate to the road conditions and user driving mode. We intend to study whether a neural network is able to find the associations required to estimate vehicle pose. To investigate if the approach can adapt to different vehicle parameters, we use a model car to safely generate data to improve the results on the full-scale test vehicle.

[a] https://orcid.org/0000-0002-1677-9245
[b] https://orcid.org/0000-0001-9895-4213
[c] https://orcid.org/0000-0001-7819-7163
[d] https://orcid.org/0000-0003-1596-7030

2 EMPLOYED PLATFORMS

2.1 Autonomous Vehicle MIG

The autonomous vehicle MIG (short for Made In Germany) is equipped with drive-by-wire technology and several different sensors (Figure 1). The sensors involved in this paper are the Applanix^{TM} POS-LV 520 navigation system and the Controller Area Network (CAN) bus data. The estimation of the vehicle's position is obtained from the Applanix navigation system. It provides the position and orientation fusing information from the integrated inertial sensors, a Distance Measuring Indicator (DMI) attached to the rear left wheel and a differential GPS. The bus provides useful data related to the status of the car, such as Wheel speeds, Car speed, Steering wheel sensor, Wheel Odometry, Brake pedal and Gas pedal.

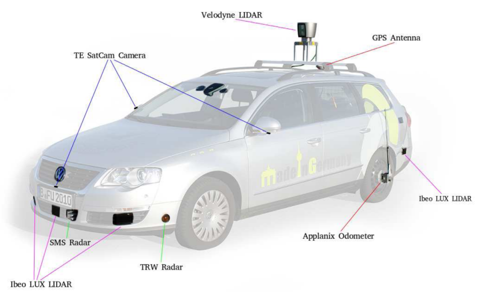

Figure 1: Overview of the Sensor Positioning on MIG autonomous vehicle.

2.2 Autominy TX1

Autominy, shown in Figure 2, is an autonomous model vehicle based on a scaled 1:10 RC car chassis, with a complete onboard system supplied with perception sensors, high computing CPU and GPU power, as well as LEDs to emulate car lights. The car runs under Ubuntu 18.04 and ROS melodic (Stanford Artificial Intelligence Laboratory et al.,). The available packages allow the car to drive autonomously and the user to read the Inertial Measurement Unit (IMU), the wheel velocities, the position of the steering wheel and the camera images.

Fig. 3a shows a graphic with the measured wheel velocities while the car is driving in circles. The mounted sensor is shown in Fig. 3b. We installed a set of three cameras on the lab ceiling to obtain ground-truth global localization.

In this work, both the MIG platform and the Autominy were used to develop the localization approach. The Autominy TX1 is particularly essential since the wheel odometry network was improved using the data generated with extreme manoeuvres, and driving manually between the limits of the localization set up in the lab.

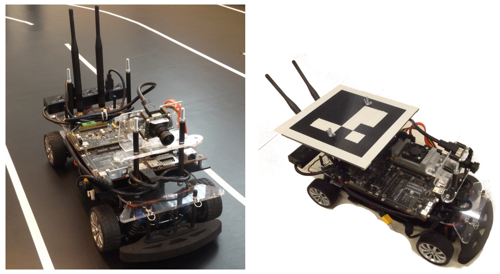

(a) (b)

Figure 2: Developed (2018) Autominy TX1 version with odometry research purposes. a) Autominy TX1 on a track made with black rubber used to achieve aggressive driving manoeuvres, The ARUCO marker in b) is used to localize the car on the track.

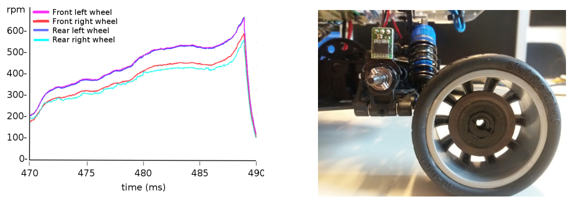

(a) (b)

Figure 3: a) Wheel Angular Velocities of Autominy TX1. Front and rear left wheels have a bigger angular velocity since the car is driving on circles counterclockwise; when the car stops, velocities drop to zero. b) The Hall sensor mounted on the car chassis and the magnetic ring installed on the wheels.

3 RELATED WORK

The Ackermann approach is derived from the geometrical assumption that the vehicle has a four-bar steering mechanism and the car moves in perfect circles which centre I is localized on the rear wheel axis and in the intersection point of the perpendicular projections from the pointing wheel direction (see Fig.4).

Moreover, in the models based on Ackermann, the mathematical approach assumes that the arc on which the car moves between origins, can be approximated up to the second-order as $\Delta = |O_k O_{k+1}|$, taking the following equations to calculate displacement with Ackermann kinematics derived from Fig.4:

$$\begin{aligned} x_{k+1} &= x_k + \Delta \cos(\theta_k + \omega/2) \\ y_{k+1} &= y_k + \Delta \sin(\theta_k + \omega/2) \\ \theta_{k+1} &= \theta_k + \omega \end{aligned} \tag{1}$$

Where x, y and θ are the 2D coordinates of the car

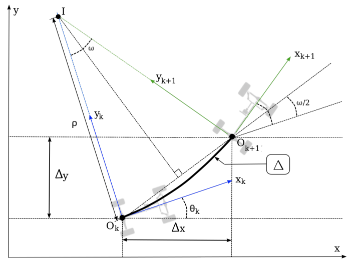

Figure 4: Ackermann steering geometry on a global frame. I is the instantaneous center of rotation between the car frames O_k and O_{k+1}, Δ is the traveled distance and ρ is the radius.

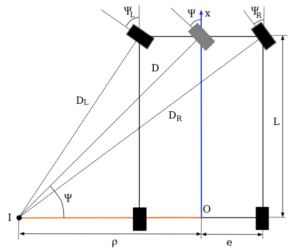

Figure 5: Geometry of the car related to the mobile frame O. Ψ is the Ackermann angle which is referenced on a middle virtual wheel, ρ is the radius, e is the half track and L the wheel-base of the vehicle.

in different k instants of time, Δ is the travelled distance, and ω is the angle between coordinate systems of the car on times k and $k+1$ related to the instantaneous centre of rotation.

In order to calculate Δ and ω, data obtained from the ABS should be used. In the most basic approach, the differential odometry can be calculated from the rear wheel displacement as follows:

$$\Delta = \frac{\delta_{RR} + \delta_{RL}}{2} \qquad \omega = \frac{\delta_{RR} - \delta_{RL}}{2e} \tag{2}$$

where δ is the linear displacement of the wheel in meters, the sub-indexes RR and RL correspond to the Rear Right wheel and the Rear Left wheel and e is the half-track of the car.

However, tire slip makes differential odometry not adequate for practical use. The Ackermann angle ψ is usually used to improve the results. Add the circle movement constraint, the radius ρ can be calculated from Fig. 5 as follows:

$$\rho = \frac{\delta_{RL}}{\omega} + e \qquad \rho = \frac{\delta_{RR}}{\omega} - e \tag{3}$$

Ackermann angle is then included on the equation list with the radius or the displacement:

$$\tan(\Psi) = \frac{L}{\rho} \qquad \tan(\Psi) = L\frac{\omega}{\Delta} \tag{4}$$

were L is the wheel-base distance of the car. It is theoretically possible to compute an Ackermann odometry using the steering angle sensor of the car to calculate ω with Eq. (4) and integrating the velocity measurements of each wheel from the ABS sensors to calculate Δ with Eq. (2).

In a vehicle the effective half-track e and the wheel-base L are not constant due to external disturbances like the suspension system, the wheel contact area with the floor which modifies the tire force and wear of the materials. Additionally, in practice, the Ackermann steering geometry of the mechanism can be changed to affect the dynamic settings of the car. In order to measure the Ackermann angle, the Steering Wheel Angle Sensor (SAS) of the car must be mapped between the wheel position and the wheel Ackermann angle.

The relationship between the steering sensor and the Ackermann angle can be approximated using the SAS ((Fejes, 2016), (Kallasi et al., 2017)). The approximation function holds just for a known working acceleration and velocity threshold, defined by the user.

Notwithstanding that the mathematical structure of the Ackermann principle is simple, the tire force is not taken into account. It is necessary since the wheels usually do not move on their heading direction. Therefore, a more precise concept of odometry must then take into account the Vehicle Slip Angle (VSA). VSA, also known as the drifting angle, is the angle between the vehicle longitudinal axis and the direction of travel, taking the centre of gravity as a reference ((Chindamo et al., 2018)). The VSA is calculated as follows:

$$\beta = -\arctan\left(\frac{v_y}{v_x}\right) \tag{5}$$

where v_x and v_y are the longitudinal and lateral velocity of the car. The VSA is widely used for stability controllers such as ESC (Yim, 2017) or VSC (Fukada, 1999), AFS (Bechtoff et al., 2016), MPC (Zanon et al., 2014), among others. Typically for such applications, an accuracy of 0.1 degrees is needed. The stability controllers regulate the tracking force of each wheel employing the brakes in the vehicle. In this way, it is possible to have a point of rotation I as close to the perpendicular projection of the centre of gravity. Therefore, in terms of localization, having such controllers help to ensure that the vehicle has a common center of rotation among the four wheels. With this assumption, a new estimation of the trajectory can be formulated.

To estimate VSA through GPS-inertial sensors, (Kiencke and Nielsen, 2000) compute the slip angle employing the bicycle model as follows:

$$\dot{\beta} = \frac{a_y}{v_g} - \dot{\psi} \tag{6}$$

where $v_g = \sqrt{v_x^2 + v_y^2}$ is the velocity of the vehicle, $\dot{\psi}$ is the yaw rate and a_y is the lateral acceleration. In this article, this approximation is used as a characteristic to train the network.

The first efforts to integrate a learning agent to the estimations fused two methods, an observer (typically an EKF) which estimates the dynamic of the car and the neural network estimates the tire data ((Acosta Reche and Kanarachos, 2017), (Dye and Lankarani, 2016)).

Most of the authors used a general approach of a three-layered neural network: the input layer, one hidden layer and the output layer. The first and second layer use log-sigmoid transfer function and a linear activation on the last layer ((Wei et al., 2016), (Broderick et al., 2009), (Li et al., 2016)).

Different state inputs to the net were evaluated. The neural network which was able to estimate a better VSA takes into account the change on dynamic parameters respect to time.

Although the VSA estimator with neural networks shows sufficient accuracy in practical applications, the main issues up to today remain in the inability of the net to adapt after the training if the vehicle parameters change and the option to deal with a road banking angle which has to be estimated with an external algorithm and then filter out the lateral acceleration component due to gravity as in (Sasaki and Nishimaki, 2000), and (Melzi et al., 2006). In (Reina et al., 2010), visual VSA has been used in non-holonomic robots to correct odometry estimations.

Neural networks and deep learning have shown their abilities to overcome analytical methods in disciplines such as time series forecasting. The application of neural network methods based on vision in vehicle localization has been widely studied ((Konda and Memisevic, 2015),(Wang et al., 2017),(Zhan et al., 2018)). However, very few studies use other sensors such as odometer, imu and GPS. (Brossard and Bonnabel, 2019) proposed a Gaussian Process combined with neural network and variations inference to improve the propagation and measurement functions, thereby improving the localization accuracy. (Belhajem et al., 2018) trained a network to learn the localization error of EKF when GPS was available and use the network for pose prediction during GPS signal outage. Different from the existing researches, we trained an end-to-end neural network to learn the VSA rate to assist the pose estimation.

4 PROPOSED METHOD

To be able to train a neural network though supervised learning, we build a dataset that stores an input array of size $nx9$ every Δ of time, being n the number of timestamps in the dataset. Each row in the matrix has the following features:

$$I = [\delta, v_{ref}, a_x, a_y, \dot{\Psi}_V, \omega_{rl}, \omega_{rr}, \omega_{fl}, \omega_{fr}] \tag{7}$$

where: δ is the steering angle, v_{ref} is the speed over ground, a_x is the longitudinal acceleration, a_y is the cross acceleration, $\dot{\Psi}_V$ is the yaw rate and ω_{xx} is the speed of the front and rear wheels.

The idea behind including just the variables in 7 and not other parameters such as constant vehicle mass, size of the wheel-base, wheel diameter or others, is that we are looking for a more complex representation of these parameters that allow the neural network to predict odometry for different size of vehicles.

Since an element of the dataset describes the instantaneous dynamic state of the car, we build the inputs of the net as a concatenated pair of vectors of 7, for instance:

$$\mathcal{X}_k = [I_i, I_{i+1}] \tag{8}$$

For the net output, we compose an array of size $nx4$, which includes the poses of the car. Instead of recording the global pose, we stored local relative poses. Local poses allow us to predict local displacements with the net.

To ease the net training, we reduced the problem to a two-dimensional trajectory. Although for two-dimensional estimation, only the *Yaw* angle to define orientation is needed, we stored the quaternion values; during training, the quaternion representation showed to help the net to converge faster. In an Euler rotation of the format ZYX, the non zero values q_z and q_w are the last two items of a quaternion. The generated vector is then as follows:

$$y_k = [x, y, q_z, q_w]$$

One crucial aspect of the data set generation is the frequency at which the data is sampled. The rate of the Autominy localization is due to the frame rate of the ceiling cameras and the post-processing algorithm, which stitch the images, detect the ARUCO markers, and calculate the position of the car. Therefore, the sampling rate of the Autominy dataset is 30Hz, while the sampling rate for the MIG dataset can be configured up to 100Hz.

In order to avoid redundant data, the reading rate in the MIG was also configured to 30Hz; in this way,

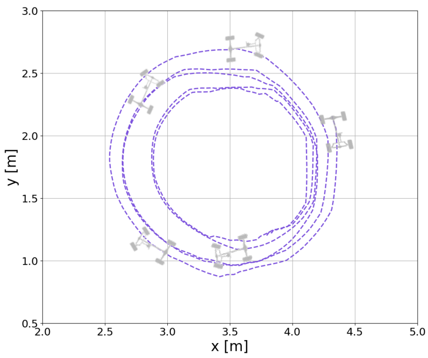

Figure 6: Autominy circle trajectory carried out with the same steering angle while increasing velocity, which developed high VSA and VSA rates.

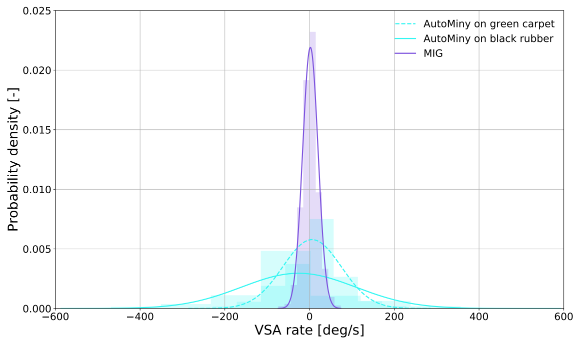

Figure 7: Range of VSA rates ($\dot{\beta}$) in the datasets. Autominy developed higher $\dot{\beta}$ over black rubber, while as expected, the MIG performed the smallest values.

we averaged a travelled distance of 0.5 m per timestep. We carried out a sanity check before storing the data. The sanity check verifies that the candidate vector is not similar to any of the already stored vectors through cosine similarity, which is a dimensionless measure for vectors, which are typically sparse.

$$sim(x,y) = \frac{\mathbf{x} \cdot \mathbf{y}}{\|\mathbf{x}\| \|\mathbf{y}\|} \tag{9}$$

The similarity equation 9 computes the cosine between two multidimensional vectors so that a value of zero means the vectors are perpendicular to each other, the closer the cosine value to one, the smaller the angle and the higher the match between vectors. In our experiments, this value was set to 0.9.

The sanity check also copes with periodic GPS corrections of the Applanix. Those corrections produce discrete spatial jumps up to 0.5 m. Since those jumps in a position generate a non-continuous trajectory, the dataset is sectioned every time a jump is detected. In this way, we store small continuous trajectories with local transformations instead of a long trajectory with global transformations.

4.1 Dataset Assembling

The datasets were obtained reading the recorded rosbags showed in Tables 1 and 2. Autominy was driven manually in two different trajectories, under variable dynamic behaviours. Fig. 6 shows a trajectory of the Autominy periodically increasing its velocity without changing the steering angle. The vehicle develops high VSA, which explains the change of the radius in the spiral trajectory.

Autominy data was recorded using two different surfaces, Cut Pile green carpet, and PVC black rubber. Driving on different surfaces allowed us to generate diverse, dynamic performances. While on the rubber surface, the car was able to drift easily, on carpet it was more stable on the curves. Analyzing how the dynamics of the car changes on such different surfaces is key to develop more accurate controllers and estimators. In this sense, another advantage of using scaled models is the ease of studying such properties by changing the surface conditions on the lab floor.

The dataset of the MIG was recorded in the city of Berlin on ten different expeditions. There are no recorded datasets while driving on snow or rain. Therefore, it is of our interest to expand the dynamic scope of the MIG trained network by means of including the founded associations under the Autominy dataset.

To examine the dynamic range of the datasets, it is possible to visualize the slip angle rate derived from Eq. 5. For Autominy, the Probability Distribution Function (PDF) of each friction surface is shown in Fig. 7 together to the MIG slip angle rate, considering that the available trajectories of the MIG are only recorded on asphalt, in an average velocity of 20 m/s; therefore only one PDF of slip angle rate is shown.

As shown in Fig.7, we drove the Autominy on a higher dynamical range than the MIG. The differences between the experiments, improve the accuracy of the MIG net by increasing the gamut of the data on which the net is trained. The overlapping between both ranges, allow the net to build a standard feature map between the Autominy and MIG dynamics.

In Table 1, the amount of train and validation timestamps are shown. Since on each dataset of Autominy, the trajectories are constantly repeated, the test section can be safely taken from the same file and use it to evaluate the results of the net. In the counterpart, the MIG rosbags are unique trajectories, and we are interested in leaving trajectories entirely for testing, owing to the fact that we would like to analyze how the net generalize for unseen trajectories.

Scenario	#Timestamps Train	Val.	Test	Driven length(m)
br driving	2451	817	817	285.7
br drifting	2375	791	791	216.6
gc driving	4716	1578	1578	537.9
gc drifting	3892	1291	1291	349.2
Total	13434	4477	4477	1389.4

Table 1: Recorded rosbags in Autominy over black rubber (br) and green carpet (gc). Different scenarios where used to increase the range of the dynamic parameters in the vehicle.

Scenario	#Timestamps Train	Val.	Test	Driven length(m)
FU_to_OBI	1260	314	0	2356.4
safari_online	7326	1831	0	12461.4
thielallee	0	0	3058	4795.3
eng	0	0	583	944.8
react4	1560	389	0	2853.9
reinickendorf	419	104	0	1659.5
aut7	2784	695	0	5907.6
auto8	0	0	1061	1487.9
2tegel	3084	771	0	9968.6
back2fu	1680	419	0	8326.9
Total	18113	4523	4702	50762.3

Table 2: Recorded rosbags in the MIG and the number of timestamps in the dataset. Sequences 3, 4 and 8 are used only for testing, meanwhile the rest of the sequences are divided between validation and training.

We acknowledge that the partition of the datasets into training and validation could avert some interesting dynamic information to the net if the data is indiscriminately divided; therefore, K-fold cross-validation was used to evaluate the performance of training on unseen data. The dataset was divided into four groups ($K = 4$). To train the final model, from the total timestamps in the Autominy dataset, 60% were taken for training, 20% for validation and 20% for testing. In the MIG dataset, seven sequences were divided between 80% training and 20% validation and the rest three sequences were used to test.

Each column of the resulting dataset matrix contains the mean and standard deviation of the column obtained from standardizing the data by subtracting the mean and dividing by the standard deviation. This way of representing the data is more convenient for the training of the net. The complete database is composed of 22388 samples from the Autominy and 27338 samples from the MIG.

Since the problem is treated as time-series, the dataset is not shuffled randomly. Instead, it is divided into several sequences of different sizes with different starts and endings. This data division expands the learning dataset, in an analogy to dataset augmentation for image-learning tasks. The initial member of each sequence is taken as the initial position of the series, and the transformations are recalculated. Nevertheless, we trained the net to learn the local transformations between timestamps. Therefore, to test the net, it is necessary to estimate the global position of the vehicle by calculating the $SE(3)$ transformation to the origin frame. It was found that feeding different sequence sizes, and shuffling such sequences each epoch, improved the performance of the net significantly. The validation and test datasets are not divided into smaller sequences, but the full sequences are estimated.

We first trained the net with the Autominy database, then, the feature map was used to train the net for the MIG.

4.2 Architecture Description

The network architecture of our Ground Autonomous Localization Net (GALNet) is shown in Fig. 8. This work utilizes Long Short Term Memory (LSTM) with a projection layer and two regression heads to estimate the slip-slip angle and localization. The LSTM exploits correlations among the time-correlated data samples in long trajectories by introducing memory gates and units (Hochreiter and Schmidhuber, 1997) in order to decrease the vanishing gradient problem (Hochreiter, 1998). Although LSTM has the ability to handle long-term dependencies, learning them is not trivial. In this work, a series of linear convolutional layers are used to extract model dynamics.

The net is represented on times k and $k+1$ to show how the states of the LSTM and SO3 layers are forward propagated to the next training step. The first two fully connected layers compute the first relationship between the dynamic variables. We use this block in the way of an encoder for the derived two outputs. In one side another dense block computes the VSA rate. The second output is made of an LSTM layer which finds the time series relationships, followed by a fully connected couple of layers that reduce the dimensionality to fit the pose output vector. The net estimates local transformation between two timestamps. Therefore, a fixed custom layer projects the displacement to a global frame.

4.3 Loss Functions

The model uses the slip angle as an auxiliary input to the pose regression. Therefore, there are two losses in the model. One to predict the correct slip angle and

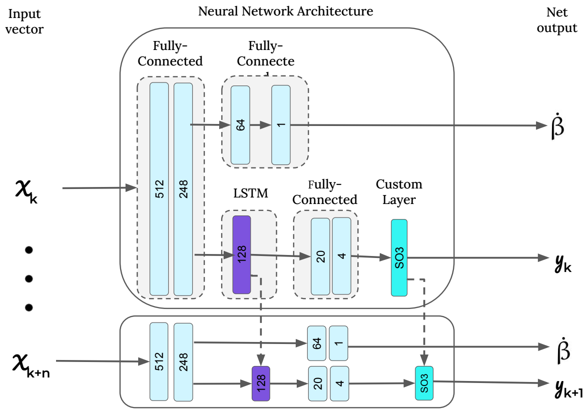

Figure 8: Architecture of GALNet.

other to regress the position. The loss regarding slip angle is as follows:

$$\mathcal{L}_{VSA} = \frac{1}{N}\sum_N \|x_n - \widehat{x}_n\|_1 \tag{10}$$

where N is the size of the batch.

The proposed method can be considered to compute the conditional probability of the poses $\mathbf{Y}_k = (\mathbf{y}_1, ..., \mathbf{y}_k)$ given a sequence of vector 7 in time t

$$p(\mathbf{Y}_t|\mathbf{X}_t) = p(\mathbf{y}_1, ..., \mathbf{y}_k|\mathbf{x}_1, ..., \mathbf{x}_k)$$

In order to maximize the previous equation, the parameters of the net can be found based on Mean Square Error (MSE). The Euclidean distance between the ground truth pose $\mathbf{y}_k = (\mathbf{p}_k^T, \Phi_k^T)$ and its estimate $\widehat{\mathbf{y}}_k = (\hat{\mathbf{p}}_k^T, \widehat{\Phi}_k^T)$ at time k can be minimized by

$$\mathcal{L}_{POS} = \frac{1}{|N|}\sum_N \|\widehat{\mathbf{x}}_k - \mathbf{x}_k\|_2 + \kappa \left\| \widehat{\mathbf{q}}_k - \frac{\mathbf{q}_k}{\|\mathbf{q}_k\|} \right\|_2 \tag{11}$$

The factor κ scales the loss between euclidean distance and orientation error to be approximately equal. $\mathbf{q}$ is in quaternion representation in order to avoid problems of Euler singularities in the global coordinate frame. Therefore the set of rotations lives on the unit sphere. During training, the values of $\widehat{\mathbf{q}}$ and $\mathbf{q}$ become close enough to be negligibly compared to the euclidean distance. Consequently, the constant κ play an essential role in the accuracy of the net. As a preliminary setting, we use the approach of (Kendall et al., 2015) where a constant κ was tuned using grid search.

Nevertheless, we observed that the error in orientation and position was related not only to κ but also with VSA rate. Selecting a constant κ value with low orientation error in small VSA rates ($\dot{\beta}$), increased the orientation error on high VSA rates. When a new

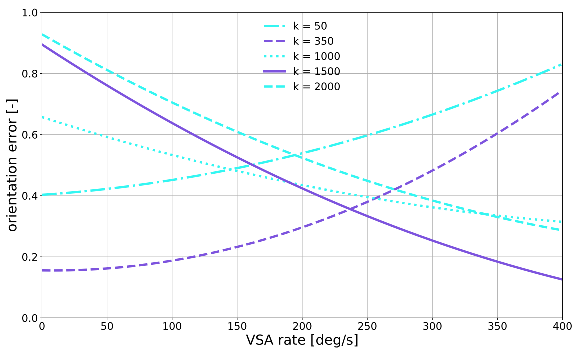

Figure 9: Orientation error for different values of κ related to the VSA rate ($\dot{\beta}$). Best values of κ for low and high $\dot{\beta}$ are showed in purple.

value was tested for high $\dot{\beta}$, the orientation error increased for low VSA rates. Fig.9 shows an iteration of κ values related to the associated VSA rate. Best value for almost zero $\dot{\beta}$ was found in $\kappa = 350$ while the best value for the higher rates (400 deg/s) was found to be around $\kappa = 1500$.

This results lead to the idea of a self-tuned κ depending on $\dot{\beta}$ which is as shown on Fig. 8 also predicted by the net. In order to adapt the scale value, a Gaussian function is proposed as follows:

$$\kappa(\dot{\beta}) = b - ae^{-(\dot{\beta}-\mu)^2/2\sigma^2} \tag{12}$$

where κ is the loss scale value, $\dot{\beta}$ is the VSA rate. b shift vertically the function in order to get the minimum value of κ when $\dot{\beta}$ is close to zero. a is the amplitude of the function, σ is the standard deviation and μ the mean of the normal distribution. σ and μ are tuned looking for the smaller orientation error with respect to $\dot{\beta}$. For the experiments, best values where found around $a = 2300$, $b = 2000$, $\mu = 0$ and $\sigma = 320$.

The final position regressor layer is randomly initialized so that the norm of the weights corresponding to each position dimension was proportional to that dimension's spatial extent.

Since the MIG database is more extent in the number of samples, the first net was trained using only this database. In order to train the Autominy net, the same architecture was used. To achieve better accuracy, the feature map of the previously trained GALNet for MIG was used, the layer group which determines the dynamic parameters is removed, as well as the last layer which composes the relative movement.

Finally, the feature map obtained from the second training is used to fine-tune the MIG net model. This exploits the associations made by the agent under the training in the Autominy dataset.

5 EXPERIMENTAL RESULTS

In this section, we briefly summarise the results of the proposed architecture for dynamic ground localization. We employ the Absolute Trajectory Error (ATE) and Relative Pose Error (RPE) metrics proposed in (Sturm et al., 2012).

5.1 Evaluation Algorithms

In order to evaluate the proposed model, we compared the results with two analytical methods.

The first algorithm is an Ackermann model odometry which is based on the wheel velocities, and an estimated Yaw rate obtained from the MIG's ABS subsystem. Originally, only the differential velocities of the back wheels were used in the MIG to determine the direction and displacement of the car; the major drawback of the differential odometry was that the wheel ticks have a systematic error that depends, among other things, on the wheel pressure, this physical event provoked the estimated trajectory to drift. In order to compensate for the deviation, the yaw rate information from MIG's ABS subsystem was involved. For the results section of this article, we identify this Ackermann-compensated differential odometry as WO.

The second algorithm is a self-implemented Unscented Kalman filter (UKF) estimator which integrates the WO and IMU measurements from the car inertial unit. The filter is obtained employing the ROS robot-localization package (Moore and Stouch, 2014).

The net was first trained on the MIG dataset, and the feature map was then used to train the net with the Autominy dataset. We differentiate the networks in the evaluation as GALNet and iGALNet correspondingly.

5.2 Quantitative Evaluation of Trajectories

In order to measure the errors on the final trained neural network, Table 3 shows the performance of the net with the ATE metric and Table 4 shows the RPE for the MIG trajectories.

Table 3 shows that in some trajectories GALNet and iGALNet improve the baseline methods. It is interesting to notice that not in all cases iGALNet performs better than GALNet, which means some associations are lost in the over-training process.

Table 4 shows that for the MIG, local displacements are still better estimated with WO. This result is expected since most of the short trajectories that are sampled at 30 Hz and have a mean displacement of 0.5 m are straight trajectories. Therefore, integration of the angular wheel velocity is still a better approximation for straight driving. WO has its major disadvantage on estimating orientation. In a global trajectory, orientation errors are collaterally translated to translational errors. For that reason, wheel odometry performs worse with the ATE metric. For some datasets, the precision of the UKF is achieved with the proposed methods.

Because the net was trained to estimate displacement between two consecutive relative positions, it is interesting to examine the RPE metric deeper and observe how the error develops since the GPS adjustments are represented as outliers. For this analysis, we selected the Safari trajectory. Fig. 10 and 11 show the RPE violin histograms of the translational and rotational components of the relative transformations.

Fig. 10 corroborates the values in Tab. 3, where

Method	Wo	UKF	GALNet	iGALNet
FU_to_OBI	86.87	**42.51**	88.48	43.43
safari_online	428.31	**4.60**	483.21	50.00
thielallee	55.97	13.84	199.5	**11.87**
englerallee	132.07	167.5	**9.20**	46.61
react4	24.33	19.10	67.65	**10.39**
reinickendorf	6.47	3.65	2.84	**2.46**
auto7	211.96	17.97	89.86	**12.36**
auto8	17.35	**3.73**	46.73	4.62
tegel	269.55	**4.48**	219.55	23.72
back2fu	506.92	**7.15**	126.48	18.33

Table 3: ATE translational error in meters of the MIG dataset before and after including the Autominy dataset in the training. The methods used to compare are: MIG Wheel Odometry (WO), Unscented Kalman Filter (UKF), GALNet trained only with the MIG dataset, and the improved version (IGALNet) trained with the Autominy dataset.

Method	Wo	UKF	GALNet	iGALNet
FU_to_OBI	**0.43**	0.49	0.71	0.59
safari_online	**0.27**	0.28	1.26	0.45
thielallee	**0.41**	0.51	0.79	0.60
englerallee	**0.44**	0.58	0.77	0.74
react4	**0.43**	0.49	0.70	0.55
reinickendorf	**0.51**	0.63	0.70	0.65
auto7	**0.39**	0.48	0.89	0.60
auto8	0.31	0.28	0.42	**0.27**
tegel	**0.95**	1.09	1.49	1.34
back2fu	**2.77**	3.09	4.04	3.13

Table 4: RPE translational error in meters of the MIG dataset before and after including the Autominy dataset in the training. The methods used to compare are: Mig wheel Odometry (WO), Unscented Kalman Filter (UKF), GALNet trained only with the MIG dataset and the improved version (iGALNet) trained with the Autominy dataset.

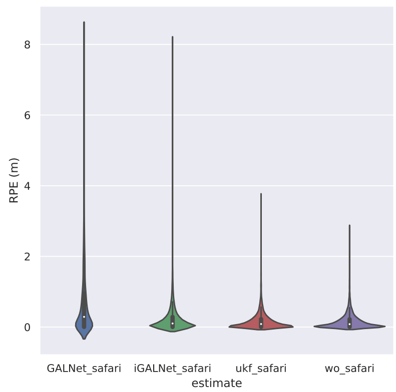

Figure 10: RPE violin histogram of the translational errors in meters in the Safari trajectory.

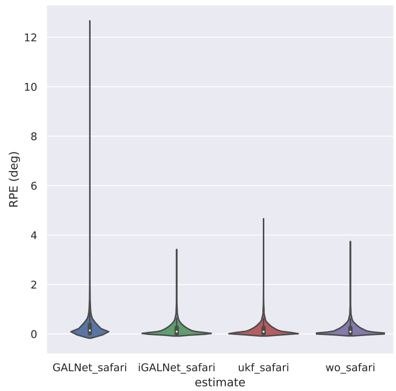

Figure 11: RPE violin histogram of the rotational errors in degrees in the Safari trajectory.

the WO estimates more effectively the translational displacement, while its biggest error is around 3 m the iGALNet goes up to 9 m, the errors accumulate closer to zero than the other algorithms. It also shows the improvement of iGALNet against GALNet. Even that the purpose of training on the Autominy dataset was to reduce rotational error focusing on VSA, translational error improved as well. However, this result suggests that a pure translational displacement dataset, generated with the Autominy could help the estimation.

In Fig. 11, the reduction of outliers between GALNet and iGALNet is more evident. The proposed deep neural network has a better rotational performance than the evaluation algorithms, which was the purpose of this work. The iGALNet network has the smallest outliers and its error distribution closer to zero than the rest of the algorithms.

The resemblance between the violin distributions of the different algorithms shows that the proposed neural network was able to find the correct associations to estimate composed displacement.

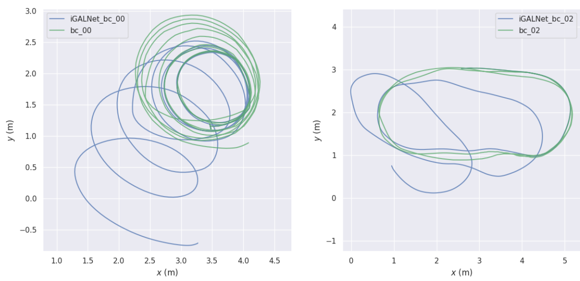

(a) (b)

Figure 12: a) Seq. 00 of the Autominy dataset, translational errors are: ATE=1.37 RPE=0.03. b) Seq. 02 of the Autominy dataset, translational errors are: ATE=2.16 RPE=0.01. On the green the ground truth obtained with the ceiling cameras in the lab, in blue, the estimated trajectory of iGALNet.

5.3 Qualitative Evaluation of Trajectories

Although the net was able to improve for small $\dot{\beta}$ and therefore contribute to the precision in the MIG dataset, the high rates in the Autominy dataset showed limited precision. Fig. 12 shows two trajectories driven in the lab with Autominy where $\dot{\beta}$ values went up to 1.2 rad/s.

Figure 13 shows the trajectories of the MIG wheel odometry, UKF and GALNet before and after (iGALNet) being trained with the Autominy dataset in Thielallee, the official test area of the MIG in Berlin. Fig. 14 - 16 show the rest of the resulting trajectories in the MIG dataset, which give a more visual evaluation of them.

5.4 Reported Runtime

The network is implemented based on the TensorFlow framework and trained using an NVIDIA Geforce RTX 2080 ti. Adam optimizer is employed to train the network with starting learning rate 0.001 and parameters $\alpha_1 = 0.9$ and $\alpha_2 = 0.999$ both values recommended on the analysis in (Kingma and Ba, 2014). The training was set for 200 epochs but using callback Tensorflow implementations such as early stopping if the loss function does not decrease 0.001 for more than five epochs to reduce the training time.

Training time on all the trajectories takes approximately 10k to 50k iterations or 2 hours to 6 hours. Prediction time for an input vector pair takes on average 25 ms, i.e., 40Hz.

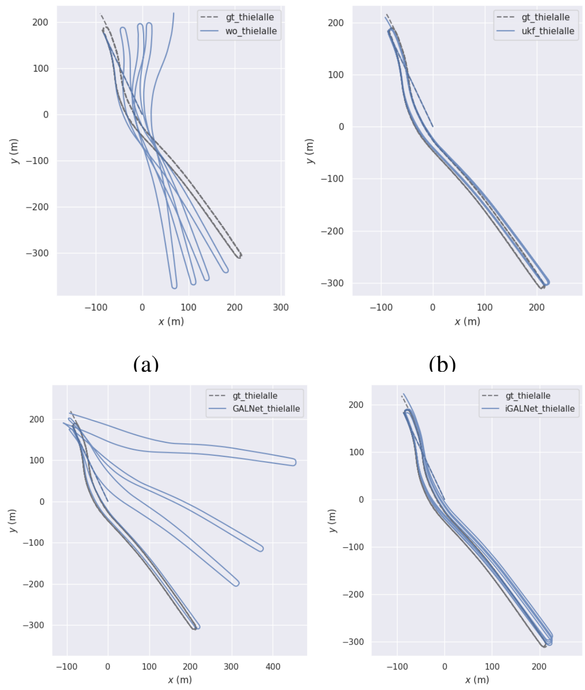

(a) (b) (c) (d)

Figure 13: Resulting trajectories of the proposed methods in Thielallee. a) MIG wheel odometry, b) UKF wheel-inertial odometry, c) GALNet, d) iGALNet.

6 CONCLUSIONS

We introduced GALNet, a deep learning architecture for pose estimation employing inertial, kinematic, and wheel velocity data from the car. We employed VSA rate as the main characteristic to estimate vehicle displacements.

We showed that it is possible to use the experiments performed by different vehicles to improve the results of the deep neural network model. The results of the estimation were compared with a Classical Unscented Kalman Filter predictor and a basic wheel odometry scheme. Transferring learning between two different experimental platforms brings advantages to the accuracy of the net. However, the model is highly dependent on the sensor, which provides ground truth, and the intrinsic drifting of the device is also transferred to the model.

The proposed method shows that, with enough information, a robust net can be trained. The performance of the net is information-dependent. If the characteristics of the dynamic system changes, the estimated position could be improved with more data collection. Therefore the system could be refined online on a test vehicle and update the weights of the net to avoid wide drifting errors.

We showed that it is possible to increment the accuracy of the models by complementing the dataset. Implementing a model that can integrate more information to improve the learning process during driving is a direction for future work.

REFERENCES

Acosta Reche, M. and Kanarachos, S. (2017). Tire lateral force estimation and grip potential identification using neural networks, extended kalman filter, and recursive least squares. *Neural Computing and Applications*, 2017:1–21.

Bechtoff, J., Koenig, L., and Isermann, R. (2016). Cornering stiffness and sideslip angle estimation for integrated vehicle dynamics control. *IFAC-PapersOnLine*, 49(11):297 – 304. 8th IFAC Symposium on Advances in Automotive Control AAC 2016.

Belhajem, I., Maissa, Y. B., and Tamtaoui, A. (2018). Improving low cost sensor based vehicle positioning with machine learning. *Control Engineering Practice*, 74:168–176.

Broderick, D., Bevly, D., and Hung, J. (2009). An adaptive non-linear state estimator for vehicle lateral dynamics. pages 1450–1455.

Brossard, M. and Bonnabel, S. (2019). Learning wheel odometry and imu errors for localization. In *2019 International Conference on Robotics and Automation (ICRA)*, pages 291–297. IEEE.

Chindamo, D., Lenzo, B., and Gadola, M. (2018). On the vehicle sideslip angle estimation: A literature review of methods, models, and innovations. *Applied Sciences*, 8(3).

Dye, J. and Lankarani, H. (2016). Hybrid simulation of a dynamic multibody vehicle suspension system using neural network modeling fit of tire data. page V006T09A036.

Fejes, P. (2016). Estimation of steering wheel angle in heavy-duty trucks.

Fukada, Y. (1999). Slip-angle estimation for vehicle stability control. *Vehicle System Dynamics*, 32(4-5):375–388.

Hochreiter, S. (1998). The vanishing gradient problem during learning recurrent neural nets and problem solutions. *International Journal of Uncertainty, Fuzziness and Knowledge-Based Systems*, 6:107–116.

Hochreiter, S. and Schmidhuber, J. (1997). Long short-term memory. *Neural computation*, 9:1735–80.

Kallasi, F., Rizzini, D. L., Oleari, F., Magnani, M., and Caselli, S. (2017). A novel calibration method for industrial agvs. *Robotics and Autonomous Systems*, 94:75 – 88.

Kendall, A., Grimes, M., and Cipolla, R. (2015). Convolutional networks for real-time 6-dof camera relocalization. *CoRR*, abs/1505.07427.

Kiencke, U. and Nielsen, L. (2000). Automotive control systems: For engine, driveline, and vehicle. *Measurement Science and Technology*, 11(12):1828–1828.

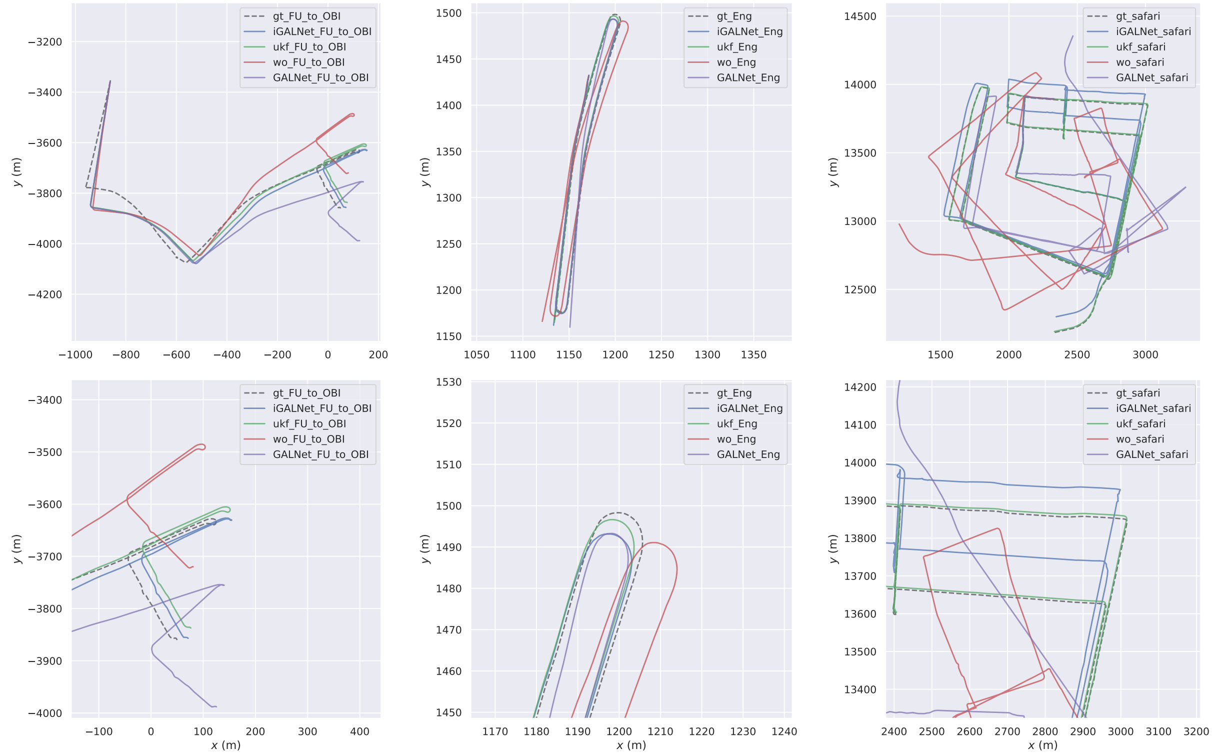

Figure 14: Trajectories in datasets FU_to_OBI, Englerallee and safari_online, showing complete and close up of them.

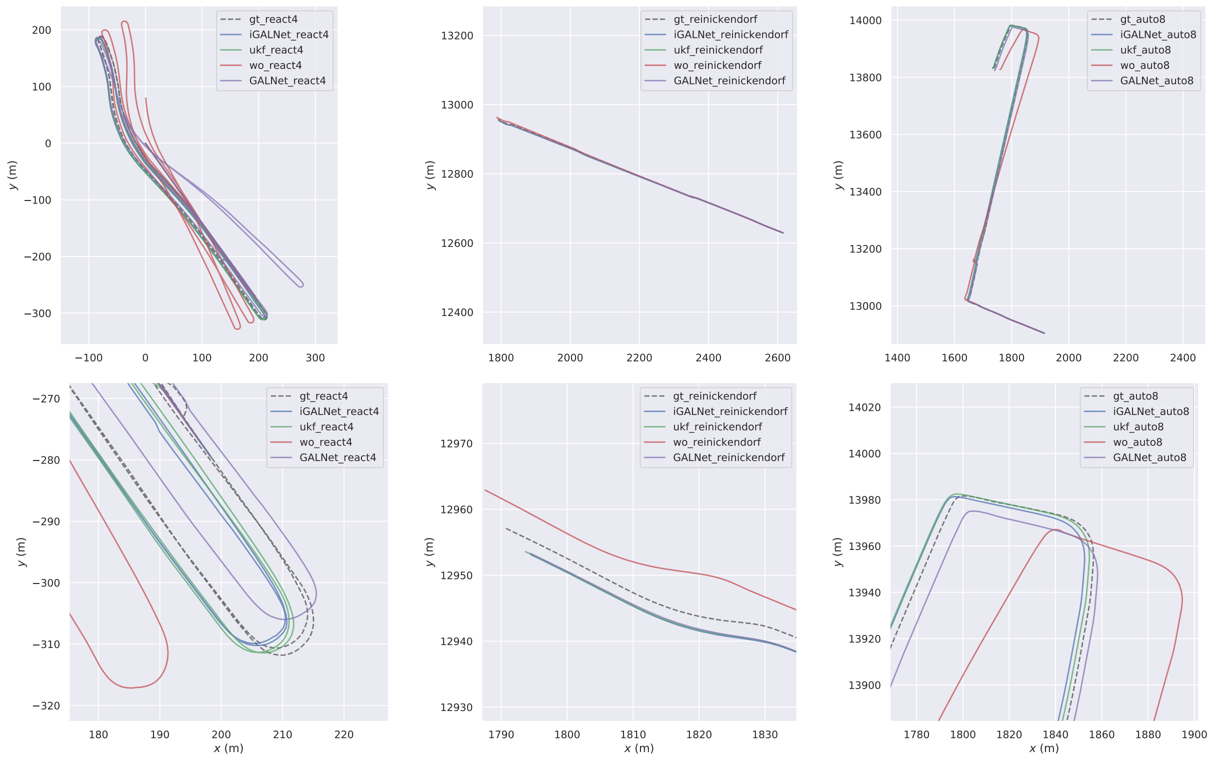

Figure 15: Trajectories in datasets react4, reinickendorf and auto8.

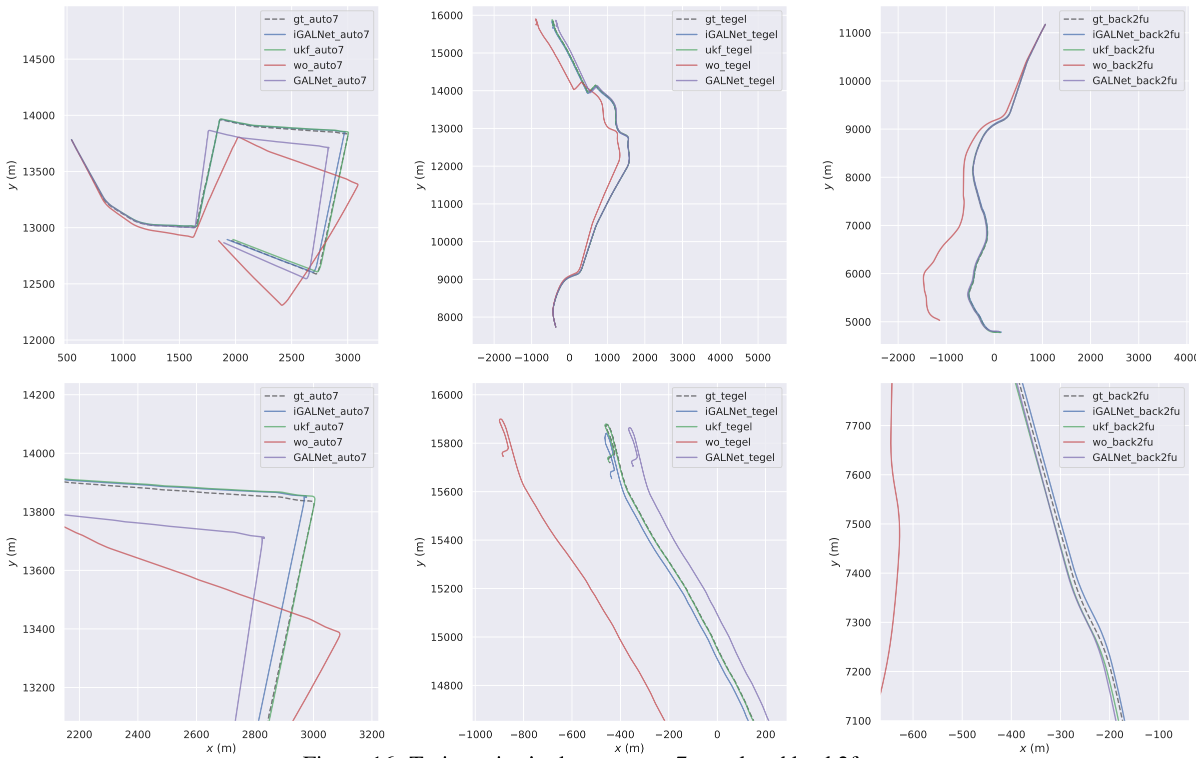

Figure 16: Trajectories in datasets auto7, tegel and back2fu.

Kingma, D. P. and Ba, J. (2014). Adam: A method for stochastic optimization.

Konda, K. R. and Memisevic, R. (2015). Learning visual odometry with a convolutional network. In *VISAPP (1)*, pages 486–490.

Li, Z., Wang, Y., and Liu, Z. (2016). Unscented kalman filter-trained neural networks for slip model prediction. *PloS one*, 11:e0158492.

Melzi, S., Sabbioni, E., Concas, A., and Pesce, M. (2006). Vehicle sideslip angle estimation through neural networks: Application to experimental data.

Moore, T. and Stouch, D. (2014). A generalized extended kalman filter implementation for the robot operating system. In *Proceedings of the 13th International Conference on Intelligent Autonomous Systems (IAS-13)*. Springer.

Reina, G., Ishigami, G., Nagatani, K., and Yoshida, K. (2010). Odometry correction using visual slip angle estimation for planetary exploration rovers. *Advanced Robotics*, 24:359–385.

Sasaki, H. and Nishimaki, T. (2000). A side-slip angle estimation using neural network for a wheeled vehicle. *SAE Transactions*, 109:1026–1031.

Stanford Artificial Intelligence Laboratory et al. Robotic operating system.

Sturm, J., Engelhard, N., Endres, F., Burgard, W., and Cremers, D. (2012). A benchmark for the evaluation of rgb-d slam systems. pages 573–580.

Valente, M., Joly, C., and de La Fortelle, A. (2019). Deep sensor fusion for real-time odometry estimation.

Wang, S., Clark, R., Wen, H., and Trigoni, N. (2017). Deepvo: Towards end-to-end visual odometry with deep recurrent convolutional neural networks. In *2017 IEEE International Conference on Robotics and Automation (ICRA)*, pages 2043–2050.

Wei, W., Shaoyi, B., Lanchun, Z., Kai, Z., Yongzhi, W., and Weixing, H. (2016). Vehicle sideslip angle estimation based on general regression neural network. *Mathematical Problems in Engineering*, 2016:1–7.

Weinstein, A. and Moore, K. (2010). Pose estimation of ackerman steering vehicles for outdoors autonomous navigation. pages 579 – 584.

Yim, S. (2017). Coordinated control of esc and afs with adaptive algorithms. *International Journal of Automotive Technology*, 18(2):271–277.

Zanon, M., Frasch, J., Vukov, M., Sager, S., and Diehl, M. (2014). *Model Predictive Control of Autonomous Vehicles*, volume 455.

Zhan, H., Garg, R., Saroj Weerasekera, C., Li, K., Agarwal, H., and Reid, I. (2018). Unsupervised learning of monocular depth estimation and visual odometry with deep feature reconstruction. In *Proceedings of the IEEE Conference on Computer Vision and Pattern Recognition*, pages 340–349.